

# Optical patterning of features with spacing below the far-field diffraction limit using absorbance modulation

Farhana Masid,<sup>1</sup> Trisha L. Andrew,<sup>2</sup> and Rajesh Menon<sup>1,\*</sup>

<sup>1</sup>Department of Electrical and Computer Engineering, University of Utah, Salt Lake City, Utah 84112, USA

<sup>2</sup>Department of Chemistry, University of Wisconsin-Madison, Madison, Wisconsin 53706, USA

\*[rmenon@eng.utah.edu](mailto:rmenon@eng.utah.edu)

**Abstract:** Absorbance modulation is an approach that enables the localization of light to deep sub-wavelength dimensions by the use of photochromic materials. In this article, we demonstrate the application of absorbance modulation on a transparent (quartz) substrate, which enables patterning of isolated lines of width 60nm for an exposure wavelength of 325nm. Furthermore, by moving the optical pattern relative to the sample, we demonstrate patterning of closely spaced lines, whose spacing is as small as 119nm.

©2013 Optical Society of America

OCIS codes: (110.4235) Nanolithography; (220.4241) Nanostructure fabrication.

---

## References and links

1. E. Abbé, "Beitrag zur Theorie des Mikroskops und der mikroskopischen Wahrnehmung," *Arch. Mikrosk. Anat. Entwickl. Mech.* **9**(1), 413–418 (1873).
2. E. A. Ash and G. Nicholls, "Super-resolution aperture scanning microscope," *Nature* **237**(5357), 510–512 (1972).
3. E. Betzig, J. K. Trautman, T. D. Harris, J. S. Weiner, and R. L. Kostelak, "Breaking the diffraction barrier - optical microscopy on a nanometric scale," *Science* **251**(5000), 1468–1470 (1991).
4. L. Novotny, B. Hecht, and D. Pohl, "Implications of high resolution to near-field optical microscopy," *Ultramicroscopy* **71**(1-4), 341–344 (1998).
5. T. Ito, M. Ogino, T. Yamanaka, Y. Inao, T. Yamaguchi, N. Mizutani, and R. Kuroda, "Fabrication of sub-100nm patterns using near-field mask lithography with ultra-thin resist process," *J. Photopolym. Sci. Technol.* **18**(3), 435–441 (2005).
6. J. Goodberlet, "Patterning 100 nm features using deep-ultraviolet contact photolithography," *Appl. Phys. Lett.* **76**(6), 667 (2000).
7. S. W. Hell, A. Engler, E. Rittweger, B. Harke, J. Engelhardt, and S. W. Hell, "Far-field optical nanoscopy," *Science* **316**(5828), 1153–1158 (2007).
8. J. Fischer, G. von Freymann, and M. Wegener, "The materials challenge in diffraction-unlimited direct-laserwriting optical lithography," *Adv. Mater.* **22**(32), 3578–3582 (2010).
9. J. T. Fourkas, "Nanoscale photolithography with visible light," *J. Phys. Chem. Lett.* **1**(8), 1221–1227 (2010).
10. L. J. Li, R. R. Gattass, E. Gershgoren, H. Hwang, and J. T. Fourkas, "Achieving  $\lambda/20$  resolution by one-color initiation and deactivation of polymerization," *Science* **324**(5929), 910–913 (2009).
11. T. F. Scott, B. A. Kowalski, A. C. Sullivan, C. N. Bowman, and R. R. McLeod, "Two-color single-photon photoinitiation and photoinhibition for sub-diffraction photolithography," *Science* **324**(5929), 913–917 (2009).
12. T. Tsujioka, M. Kume, Y. Horikawa, A. Ishikawa, and M. Irie, "Super-resolution disk with a photochromic mask layer," *Jpn. J. Appl. Phys.* **36**(Part 1, No. 1B), 526–529 (1997).
13. T. Tsujioka, M. Kume, and M. Irie, "Theoretical analysis of super-resolution optical disk mastering using a photoreactive dye mask layer," *Opt. Rev.* **4**(3), 385–389 (1997).
14. T. L. Andrew, H.-Y. Tsai, and R. Menon, "Confining light to deep sub-wavelength dimensions to enable optical nanopatterning," *Science* **324**(5929), 917–921 (2009).
15. H.-Y. Tsai, H. I. Smith, and R. Menon, "Reduction of focal-spot size using dichromats in absorbance modulation," *Opt. Lett.* **33**(24), 2916–2918 (2008).
16. H.-Y. Tsai, G. M. Wallraff, and R. Menon, "Spatial-frequency multiplication via absorbance modulation," *Appl. Phys. Lett.* **91**(9), 094103 (2007).
17. R. Menon, H.-Y. Tsai, and S. W. Thomas 3rd, "Far-field generation of localized light fields using absorbance modulation," *Phys. Rev. Lett.* **98**(4), 043905 (2007).

18. R. Menon and H. I. Smith, "Absorbance-modulation optical lithography," *J. Opt. Soc. Am. A* **23**(9), 2290–2294 (2006).
  19. R. F. Pease and S. Y. Chou, "Lithography and other patterning techniques for future electronics," *Proc. IEEE* **96**(2), 248–270 (2008).
  20. S. Berning, K. I. Willig, H. Steffens, P. Dibaj, and S. W. Hell, "Nanoscopy in a living mouse brain," *Science* **335**(6068), 551 (2012).
- 

The smallest focal spot with conventional far-field optics is limited by the diffraction limit to about  $\lambda/2$ , where  $\lambda$  is the illumination wavelength [1]. This diffraction limit also constraints the resolution of features that can be patterned using optics. There are a number of approaches that have been proposed to circumvent the far-field diffraction limit. These approaches include near-field optical [2–4] or contact lithography [5], where in the maskless case, a nanoscale tip or aperture, which serves as the source of photons scans across a photosensitive material. The high spatial frequencies that are normally evanescent and hence, negligible in the far-field, can contribute to the near-field. In this case, the size of the spot is comparable to the size of the tip. Unfortunately, this size is very sensitive to the distance between the tip and the sample, and hence quite difficult to control. Furthermore, this process is serial and very slow. It is difficult to parallelize due to the challenge of maintaining the spacing between the tip and the substrate. Contact photolithography suffers from the requirement of a mask with its concomitant disadvantages. Furthermore, intimate contact across the image field that is required for high resolution is extremely challenging to achieve [6].

Alternative patterning approaches include those that exploit excitation and de-excitation photoreactions. Such approaches are closely related to stimulated-emission-depletion microscopy (STED) and related pointillist-imaging schemes [7]. In these microscopy techniques, a focused excitation beam is scanned across a sample, typically in a raster fashion. A depletion-beam pulse, which is red-shifted with respect to the excitation beam, is focused into a ring-shaped spot and closely follows the excitation beam. This depletion beam induces stimulated depletion of the excited fluorophores, thereby reducing the size of the excitation region and achieving sub-diffraction-limited imaging. It is non-trivial to extend this approach directly to nanopatterning [8]. A straightforward extension utilizes an excitation beam, which causes a photoreaction that initiates polymerization. The ring-shaped depletion-beam, then induces a de-excitation reaction, which inhibits the polymerization reaction. By controlling the region of inhibition to surround the polymerization region sufficiently, it is possible to confine polymerization to a region that is smaller than the far-field diffraction limit. In one of these methods termed resolution enhancement through photoinduced deactivation (RAPID) [9, 10], 2-photon absorption of a near-infrared laser beam initiates radical polymerization. A subsequent 1-photon absorption of a continuous wave (CW) laser at the same wavelength deactivates this polymerization reaction. When the CW beam is engineered to have a node, polymerization is restricted to a narrow region at the center. Thus, super resolution is achieved. The main disadvantage is the high intensity required to enable the 2-photon initiation of polymerization. It is difficult to parallelize this approach for high speed. Furthermore, it is challenging to achieve macro-molecular (sub-10nm) resolution with polymerization reactions. The nanoscale pattern is created by dissolving away the monomer bulk, while leaving the polymerized regions behind. A certain length of the polymer chain is necessary to create this solubility difference, which limits the smallest region that can be reliably patterned. Another approach uses single-photon reactions during both photoinitiation and photoinhibition of polymerization [11]. A focused spot at one wavelength initiates polymerization while a subsequent focused node at a second wavelength inhibits polymerization. One of the major disadvantages of this approach is the poor selectivity between photoinhibition and photopolymerization. In other words, there is a non-zero probability that the second wavelength not only inhibits the polymerization but also initiates it. This leads to poor image contrast during lithography and limits the achievable resolution.

Generally speaking, those approaches that extend the ideas of STED directly to patterning require a photosensitive material that is not only a good photoresist but also has to exhibit wavelength-specific photoswitchable properties. This is a challenging materials problem [8]. An alternative approach is to separate the photoswitching from the recording properties. In other words, a separate layer placed on top of the photoresist can be used as the photo-switchable medium. A related approach was demonstrated in optical memories previously [12, 13]. Our approach, which we refer to as absorbance modulation, requires the simultaneous exposure with a focused bright spot at the exposing wavelength ( $\lambda_1$ ) and a focused ring-shaped spot at a non-exposing wavelength ( $\lambda_2$ ) [14–18]. As illustrated in Fig. 1(a), the photo-switchable material, which forms what we call the absorbance-modulation layer (AML), inter-converts between an absorbing isomer and a transparent isomer by exposure to  $\lambda_1$  and  $\lambda_2$ , respectively. In Fig. 1(b), we illustrate the exposure in 1-dimension, where the sample is exposed to two standing waves. The period of the standing wave at  $\lambda_1$  is half that at  $\lambda_2$ . When the AML absorbs a photon of wavelength  $\lambda_1$ , it converts into the transparent form. On the other hand, when the AML absorbs a photon of wavelength  $\lambda_2$ , it converts back into the opaque form. The combination of exposures from the two wavelengths produces a sub-diffraction-limited transparent region, through which photons of wavelength  $\lambda_1$  penetrate, and expose the photoresist underneath. In this case, one can optimize the AML separately from the photoresist. In other words, the AML can be chosen to provide the best photo-switchable properties, while the photoresist can be optimized to serve as a good etch mask, for instance. Previously, we demonstrated isolated features with widths as small as  $\sim\lambda_1/10$  using this technique [14]. As indicated in Fig. 1(b), a barrier layer comprised of polyvinylalcohol (PVA) is necessary to protect the photoresist from the overlying AML. After exposure, the AML and the PVA layers must both be removed prior to development as illustrated in Figs. 1(c) and 1(d). This can potentially be damaging to the photoresist. In this article, we propose a new technique, which avoids this extra step and hence, allows for a more benign processing of the photoresist.

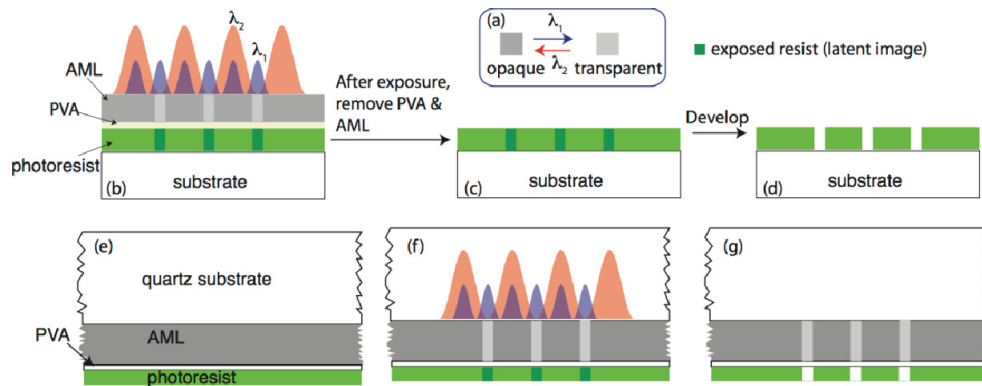


Fig. 1. Schematic of absorbance-modulation-optical lithography (AMOL) based on photo-switching of the AML (a) using the conventional process (b)-(d) and using the new process (e)-(g).

The new process is shown schematically in Figs. 1(e)-1(g). The substrate is comprised of a quartz slide that is transparent to both wavelengths of interest. The quartz substrate is first cleaned by using a mixture of  $\text{NH}_4\text{OH}:\text{H}_2\text{O}_2:\text{H}_2\text{O}$  (1:1:5) at  $80^\circ\text{C}$  for 30mins. HMDS is then spun-cast at 6000rpm for 60s and air-dried for 10minutes. This serves as an adhesion promotion layer. The AML is comprised of 1,2-bis[2-methyl-5-(5'-methyl-2'-thienyl)-3-thienyl]hexafluorocyclopentene (**BTE**) mixed into a 30 mg/mL solution of PMMA in anisole at a 95 weight-percent loading. Then, the AML is spun-cast at 1000rpm for 3s and 500rpm for 60s. After baking the sample in an oven at  $110^\circ\text{C}$  for 60 minutes, the AML forms a layer of

thickness 410nm, which we verified with a surface profiler. Then a solution of PVA in water at concentration of 1:4.4 by weight is spun-cast at 3000rpm for 60s. Upon baking the sample in an oven at 80°C for 5 minutes, the PVA forms a layer of thickness 12nm. A second layer of HMDS is spun-cast on the PVA layer at 6000rpm for 60s to improve adhesion to the last photoresist layer. The sample is air-dried for 10 minutes. Finally, a solution of Shipley 1813 photoresist thinned down with type-P thinner to a concentration of 1:11 by weight is spun-cast at 2000rpm for 60s. After baking the sample in an oven at 110°C for 15 minutes, the photoresist forms a layer of thickness 50nm. Exposure is performed through the quartz substrate as illustrated in Fig. 1(f). The exposure system is a modified Lloyd's-mirror interferometer that utilizes two laser wavelengths as illustrated in Fig. 2(a). A standing wave of period  $\sim 280$  nm was formed at a wavelength,  $\lambda_1 = 325$ nm and a standing wave of period  $\sim 570$  nm was formed at a wavelength,  $\lambda_2 = 647$ nm. The intensity of the  $\lambda_1$  beam was  $\sim 4\mu\text{W}/\text{cm}^2$  and that of the  $\lambda_2$  beam was  $\sim 54\text{mW}/\text{cm}^2$ . After exposure, the sample was developed directly without any intervening process steps as illustrated in Fig. 1(g).

An atomic force micrograph of the developed photoresist surface is shown in Fig. 2(b). Note that lines of width as small as 60nm are clearly resolved. This corresponds to  $\lambda_1/5.4$ . The far-field diffraction limit is given by half the period of the standing wave at  $\lambda_1$ , *i.e.*, 140nm. It is important to point out that the  $\lambda_2$  photons do not have sufficient energy to expose the photoresist. Nevertheless, the lines are spaced by the period of the  $\lambda_2$  standing wave as expected by the illustration in Fig. 1(f). The linewidth variation across the image field is likely due to variations in the thickness of the AML as well as some high-spatial frequency noise in the laser illumination. Better AML formulation that allows for increased solvation and uniform packing of the BTE molecules within the polymer matrix, as well as improved processing conditions (e.g., faster spin coating) will enhance the AML film quality in the future. In Fig. 2(c), we show how the linewidths change with exposure dose. As expected, the linewidth increases slowly at first and at a faster rate at higher exposure dose. This is opposite to what one would expect with a simple sinusoid intensity distribution of the  $\lambda_1$  illumination. As we have discussed earlier, absorbance modulation increases the normalized image slope (and image contrast) [18], which agrees with the linewidth-dose dependence that we observed here.

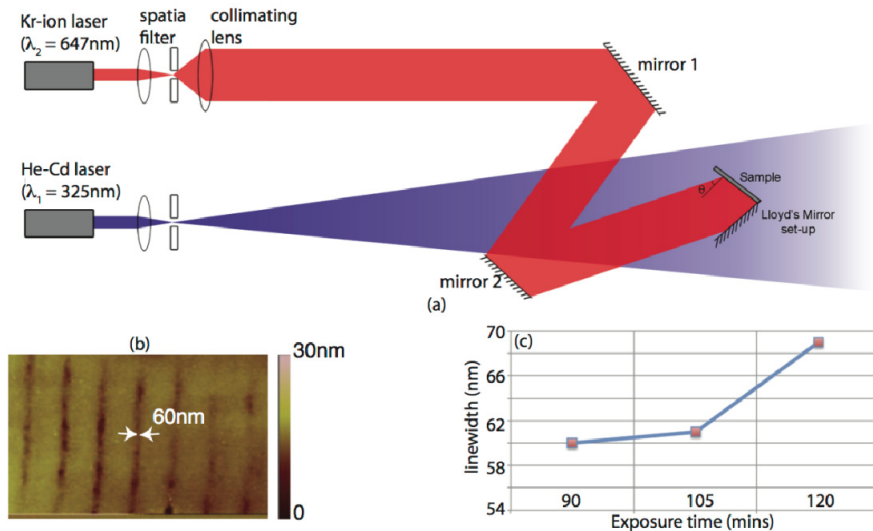


Fig. 2. (a) Illustration of the dual-wavelength Lloyd's mirror interferometer, where the sample is illuminated by two standing waves. The period of the  $\lambda_1$  standing wave is approximately half that of the  $\lambda_2$  standing wave. (b) Atomic-force micrograph of lines in developed resist after a single exposure. (c) Linewidth as a function of exposure time for single exposures.

One of the advantages of AMOL is that the AML is reversible. In other words, it is possible to do multiple exposures and avoid proximity-effects by allowing the AML to recover to its original opaque form after each exposure. This is illustrated schematically in Figs. 3(a)-3(e). The exposure was conducted as described earlier and the exposure time was  $\sim 3$  hours (Fig. 3(a)). After this exposure, the  $\lambda_1$  beam is turned off. Half the  $\lambda_2$  beam is blocked such that the sample is illuminated to a uniform beam. The sample is exposed to this uniform beam for  $\sim 3$  hours to ensure that the AML is fully converted into the opaque form as illustrated in Fig. 3(b). Then, the sample is displaced relative to its previous position. The exposure is repeated for 3 hours as shown in Fig. 3(c). This results in lines that are spaced according to the relative displacement of the sample as indicated in Fig. 3(e). The atomic-force micrograph shown in Fig. 3(f) confirms this process experimentally, where the line spacing is  $\sim 290$ nm, which is less than the period of the  $\lambda_2$  standing wave (570nm). This provides a promising approach to create closely packed features without intervening process transfer steps as is typically needed in semiconductor lithography [19].

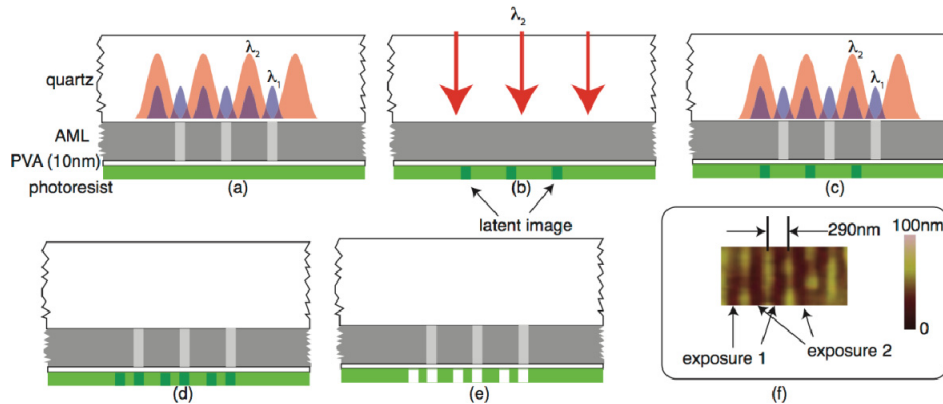


Fig. 3. Schematic of multiple exposures for patterning dense features using AMOL. (a) Exposure with standing waves at  $\lambda_2$  and at  $\lambda_1$  results in isolated lines of exposed resist. The sample is then exposed to a uniform illumination at  $\lambda_2$ , which converts the AML completely into the opaque form. The sample is stepped with respect to the optics and a second exposure with standing waves at  $\lambda_2$  and at  $\lambda_1$  is conducted. This results in dense lines as illustrated in (d) and after development in (e). (f) Atomic-force micrograph of dense lines whose approximately spacing is half that of the period of the  $\lambda_2$  standing wave.

By introducing a relative rotation between the multiple exposures, it is possible to create more complex geometries. An example with two exposures is shown in Fig. 4(a), where two exposures (6 hours each) were performed with a small rotation between the patterns. In this case, we blocked half the UV beam such that the sample was exposed to a uniform beam at  $\lambda_1$  and a standing wave at  $\lambda_2$ . The intervening exposure to only the red beam was for 4 hours. For the samples shown in Figs. 4(b) and 4(c), the AML was spun-cast at 500 rpm for 5 minutes and formed a layer of thickness  $\sim 700$ nm. The atomic-force micrographs shown in Figs. 4(b) and 4(c) show exposed regions that are spaced by a distance of 142nm and 119nm, respectively. This corresponds to  $\lambda_2/4.6$  and  $\lambda_2/5.44$ , respectively. Note that here  $\lambda_2$  is used for comparison since the  $\lambda_1$  beam is unpatterned and hence, has no spatial frequencies to contribute. These examples indicate that absorbance modulation enables patterns whose spacing can be smaller than the far-field diffraction limit of the optical system. Note that in this case, the limit is defined by the largest spatial frequency in the  $\lambda_2$  beam, which corresponds to a spacing of  $570\text{nm}/2 = 285\text{nm}$ .

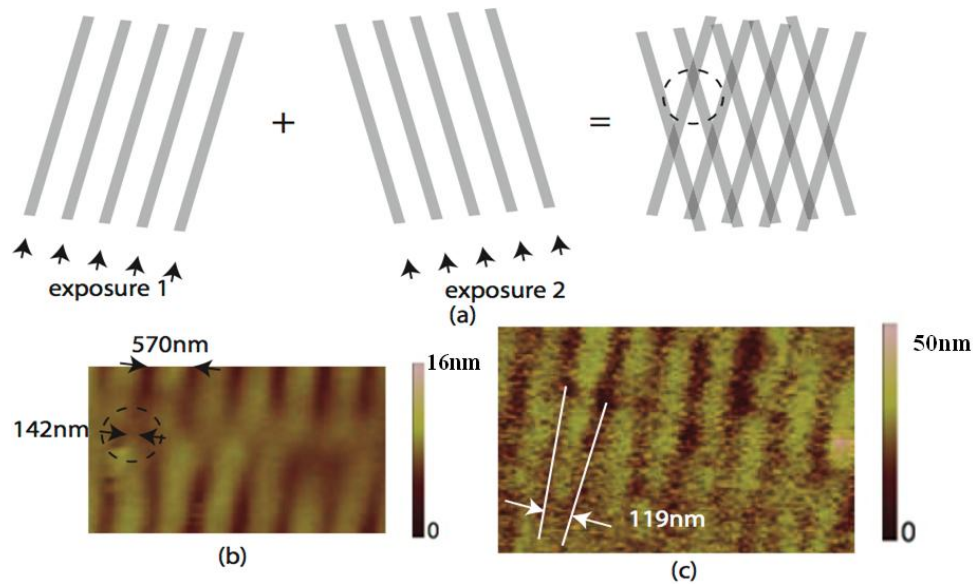


Fig. 4. (a) Schematic of a 2-step exposure, where the 2nd exposure is rotated with respect to the 1st. (b) and (c) Atomic-force micrographs of two samples that were exposed twice with a small rotation in between. Black-dashed circles show the corresponding regions.

Optics has significant advantages for high-throughput nanomanufacturing as evidenced by the ubiquitous popularity of optical-projection lithography in semiconductor manufacturing. However, the far-field diffraction limit is a fundamental physical barrier that curtails nanomanufacturing. In this article, we described preliminary results that demonstrate the feasibility of absorbance-modulation optical lithography (AMOL) as a means to multiple exposures with no intervening process steps. Further optimization of the photochromic material and the photoresist, when combined with an array of two-dimensional nodes in the  $\lambda_2$  beam can generate nanoscale patterns of complex geometries analogous to super-resolution imaging of complex distribution of fluorophores [20].

#### Acknowledgments

We would like to thank Brian Baker and Brian Van Devener of the Utah nanofabrication facility for assistance with characterizing the nanostructures. We also thank Apratim Majumder for assistance with the Lloyd's-mirror setup. Financial support from DARPA and the Utah Science, Technology and Research (USTAR) Initiative are gratefully acknowledged.